Title

Nanorod Suprastructures from a Ternary Graphene Oxide—Polymer—CsPbX3 Perovskite Nanocrystal Composite That Display High Environmental Stability

Journal

Nano Letters, 17(11)

ISSN

1530-6984

Authors

Pan, Aizhao

Jurow, Matthew J

Qiu, Fen

et al.

Publication Date

2017-11-08

DOI

10.1021/acs.nanolett.7b02959

Peer reviewed

Nanorod Suprastructures from a Ternary Graphene Oxide-Polymer-$CsPbX_3$ Perovskite Nanocrystal Composite that Display High Environmental Stability

Aizhao Pan,[†,‡] Matthew J. Jurow,[‡,#] Fen Qiu,[‡,] Juan Yang,[#] Baoyi Ren,[‡,$] Jeffrey J. Urban,[‡] Ling He,[†] Yi Liu*[‡,#]*

[†]Department of Chemistry, School of Science, Xi'an Jiaotong University, Xianning WestRoad, 28, Xi'an, 710049, China.

[‡]The Molecular Foundry, Lawrence Berkeley National Laboratory, Berkeley, California 94720, United States.

[$]Key Laboratory of Inorganic Molecule-Based Chemistry of Liaoning Province, College of Applied Chemistry, Shenyang University of Chemical Technology, Shenyang 110142, China.

[#]Materials Sciences Division, Lawrence Berkeley National Laboratory, Berkeley, California 94720, United States.

Keywords: Hybrid Materials, Nanorod, Perovskite Nanocrystals, Photoluminescence, Self-assembly

ABSTRACT

Despite the exceptional optoelectronic characteristics of the emergent perovskite nanocrystals, the ionic nature greatly limits their stability and thus restricts their potential applications. Here we have adapted a self-assembly strategy to access a rarely reported nanorod suprastructure that provide excellent encapsulation of perovskite nanocrystals by polymer-grafted graphene oxide layers. Polyacrylic acid grafted graphene oxide (GO-*g*-PAA) was used as a surface ligand during the synthesis of the $CsPbX_3$ perovskite NCs, yielding particles (5-12 nm) with tunable halide compositions that were homogeneously embedded in the GO-*g*-PAA matrix. The resulting NC-GO-*g*-PAA exhibits a higher photoluminescence quantum yield than previously reported encapsulated NCs while maintaining an easily tunable bandgap, allowing for emission spanning the visible spectrum. The NC-GO-*g*-PAA hybrid further self-assembles into well-defined nanorods upon solvent treatment. The resulting nanorod morphology imparts extraordinary chemical stability towards protic solvents such as methanol and water and much enhanced thermal stability. The introduction of barrier layers by embedding the perovskite NCs in the GO-*g*-PAA matrix, together with its unique assembly into nanorods, provides a novel strategy to afford robust perovskite emissive materials with environmental stability that may meet or exceed the requirement for optoelectronic applications.

Keywords: Graphene Oxide, Hybrids, Nanorods, Perovskite Nanocrystals, Self Assembly

AMX_3 type (A = cation, M = Pb, X = Cl, Br, I) lead halide-based perovskite nanocrystals (NCs) have attracted growing research interest recently, due to their unusual and exceptional optoelectronic characteristics, crystallographic properties and photovoltaic performance.[1-6] They have demonstrated promise in optoelectronic

applications including light-emitting devices,[7-10] lasers,[2, 7, 11] solar cells[1, 3, 4, 12, 13] and photodetectors.[14-16] Great efforts have been devoted to increasing the photoluminescence quantum yield (PLQY), decreasing spectral widths, improving colloidal dispersability, and tuning bandgaps based on composition and size.[4, 17-20] The all-inorganic perovskite nanocrystals family of the formula of $CsPbX_3$ (X=Cl, Br, I) has specifically attracted considerable attention due to superior PLQY and stability compared to the organic cation based analogues.[4, 17, 18] Nanocrystals with different morphologies, such as cubes, platelets, wires and spheres, have been obtained on a wide range of length scales by controlling the synthetic conditions and the composition of surfactant ligands.[21-25]

Colloidal perovskites NCs however present major stability issues that clouded their potential for use in large-scale applications.[26-28] Due to their ionic nature, perovskite NCs are rapidly degraded by polar solvents and environmental humidity.[26, 29-31] Notable approaches to improving NC stability include polymer encapsulation,[17, 26, 32, 33] incorporation in mesoporous silica particles,[29, 34, 35] high affinity ligands,[36-38] silicone resin,[39] and using bulky capping ligands.[14, 40, 41] Most of these examples take advantage of the hydrophobicity of the encapsulation layers. Unfortunately, many of these layers impede fundamental optoelectronic processes such as efficient photoluminescence, charge generation, transport and separation in conventional quantum dots, [39, 42, 43] and may impose similar barriers for perovskite NCs.

We have been interested in introducing functional barrier layers that not only serve as encapsulation layers, but also improve the optoelectronic properties by facilitating charge separation and migration. Graphene oxide (GO) was selected because of its excellent electrical, optical, thermal and mechanical properties.[44, 45] The impermeability of graphene oxide has enabled the fabrication of barrier films for

other applications including preventing permeation of gases and moisture.[46, 47] We thus explored the synthesis of composite materials that integrate GO nanosheets with $CsPbX_3$ perovskite NCs. In order to enhance the interaction between the nanocrystals and the encapsulation layer, GO was covalently functionalized with polyacrylic acid polymer (PAA) to form a hybrid composite material (GO-*g*-PAA), which was subsequently employed as a surface ligand to mediate the synthesis of perovskite NCs. The carboxylate terminated surface ligands contribute to facile uptake of the nanoparticle precursors by coordinating the $PbBr_2$, forming an effective nucleation point for nanocrystal growth.[48] A different perovskite NC-GO hybrid without the grafted polymer ligands has recently been prepared and shown to exhibit high photocatalytic activity towards CO_2 reduction due to enhanced charge separation.[49] NCs coupled with reduced graphene oxide (rGO) were also prepared by a hot-injection method, and demonstrated an enhanced photoresponse relative to free $CsPbBr_3$ indicating potential applications for photoelectric detection.[50] In the current study, the high concentration of carboxylate groups on the polymer is advantageous for binding the nanocrystal surface, which consequently impacts NCs growth to yield a tightly bound NC-GO-*g*-PAA hybrid material.

Here we have demonstrated the effectiveness of such an approach in generating ternary perovskite NC-GO-*g*-PAA hybrids. $CsPbX_3$ nanocrystals were successfully grown into the GO-*g*-PAA matrix with uniform and tunable NC sizes and high PLQY. Moreover, we have discovered a simple and rapid solvent induced assembly of GO based-composites into well-defined nanorod suprastructures. The resulting nanorods exhibit extraordinary stability towards protic solvents such as methanol and water, as well as enhanced thermal stability.

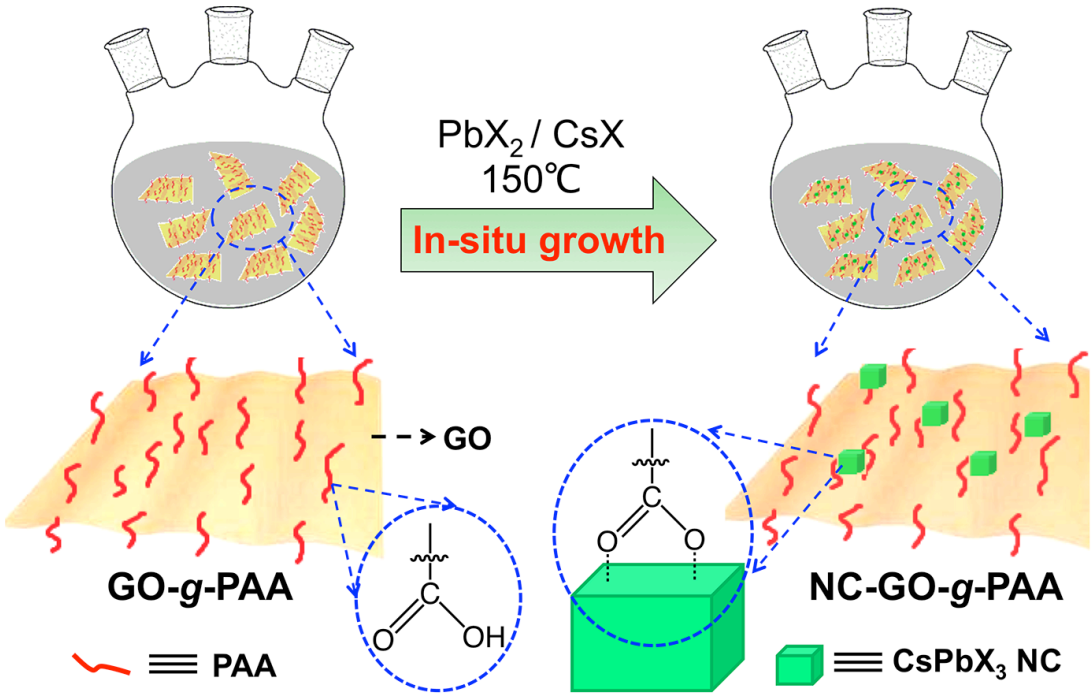

Scheme 1. Illustration of the synthesis of ternary NC-GO-*g*-PAA hybrid. The yellow sheets, the red wavy lines and the green cubes represent GO, PAA carrying free carboxylic acid groups, and perovskite nanocubes, respectively.

The synthesis of the ternary NC-GO-*g*-PAA hybrid is illustrated in Scheme 1 (see Supporting Information for full synthetic details). PAA-grafted GO (GO-*g*-PAA) was synthesized according to a reported procedure (Scheme S1).[51] Briefly, poly(*t*-butyl acrylate) (P*t*BA) was bound to GO nanosheets via a surface-initiated atom transfer radical polymerization (ATRP) reaction, followed by hydrolysis to give the GO-*g*-PAA hybrids. Two hybrids with different polymer loadings, named as GO-*g*-PAA and GO-*g*-PAA-high, were obtained by controlling the polymerization times. The grafted mass ratios of PAA brushes on the GO nanosheets are 10 and 17 wt% for GO-*g*-PAA and GO-*g*-PAA-high, respectively, as revealed by the corresponding thermogravimetric analysis (TGA) (Figure S1). Additional X-ray photoelectron spectroscopic (XPS) studies revealed a C1s peak at 288.3 eV that corresponds to the carbonyl groups in the polymer, further confirming the efficacy of the grafting

reaction (Figure S1). The ternary $CsPbX_3$ perovskite NC-GO-*g*-PAA hybrids were synthesized following a modified procedures for free $CsPbBr_3$ NCs where oleic acid was replaced with GO-*g*-PAA.[17] The obtained hybrids were then cleaned and dispersed in toluene as highly emissive colloids.

Electron microscopy was used to characterize the morphology of the NC-GO-*g*-PAA hybrid, the pristine GO and GO-*g*-PAA composite (Figures 1 and Figure S2). GO-*g*-PAA presents an ultrathin sheet-like morphology that is similar to the unfunctionalized GO, suggesting that the grafted polymer brushes on the edges and surface of GO do not alter the morphology. Scanning electron microscopy (SEM) and transmission electron microscopy (TEM) of the NC-GO-*g*-PAA hybrid revealed uniform distribution of $CsPbBr_3$ NCs embedded within the polymer functionalized GO nanosheets (Figures 1a and S3). High magnification TEM imaging (Figure 1b) shows approximately spherical nanoparticles with an average diameter of ca. 6.0±0.4 nm, distinctly different than both the larger NCs (25 nm) resulting from growth directly on the GO surface and the irregular morphologies seen in control experiments using binary systems of NC-GO and NC-PAA (Figure S4).[50] High-resolution TEM (HRTEM) studies of the NCs revealed *d* spacings of 4.1 Å and 3.4 Å (Figure 1c), corresponding to the (110) and (111) crystal lattice planes, respectively.

The bulk crystallinity of the NC-GO-*g*-PAA hybrid was then investigated by powder X-ray diffraction (PXRD) (Figure 1d) and compared against that of pristine GO and free $CsPbBr_3$ NCs. The XRD patterns of the NC-GO-*g*-PAA hybrid were consistent with the corresponding orthorhombic crystal phases of free $CsPbBr_3$ NCs (Figure 1d). The spherical morphology of perovskite NCs contrasted with the commonly observed nanocubic morphology, which is an indication of strong

influence of GO-*g*-PAA on the crystal growth of NCs, presumably through coordination between the carboxylate groups and NC surfaces.

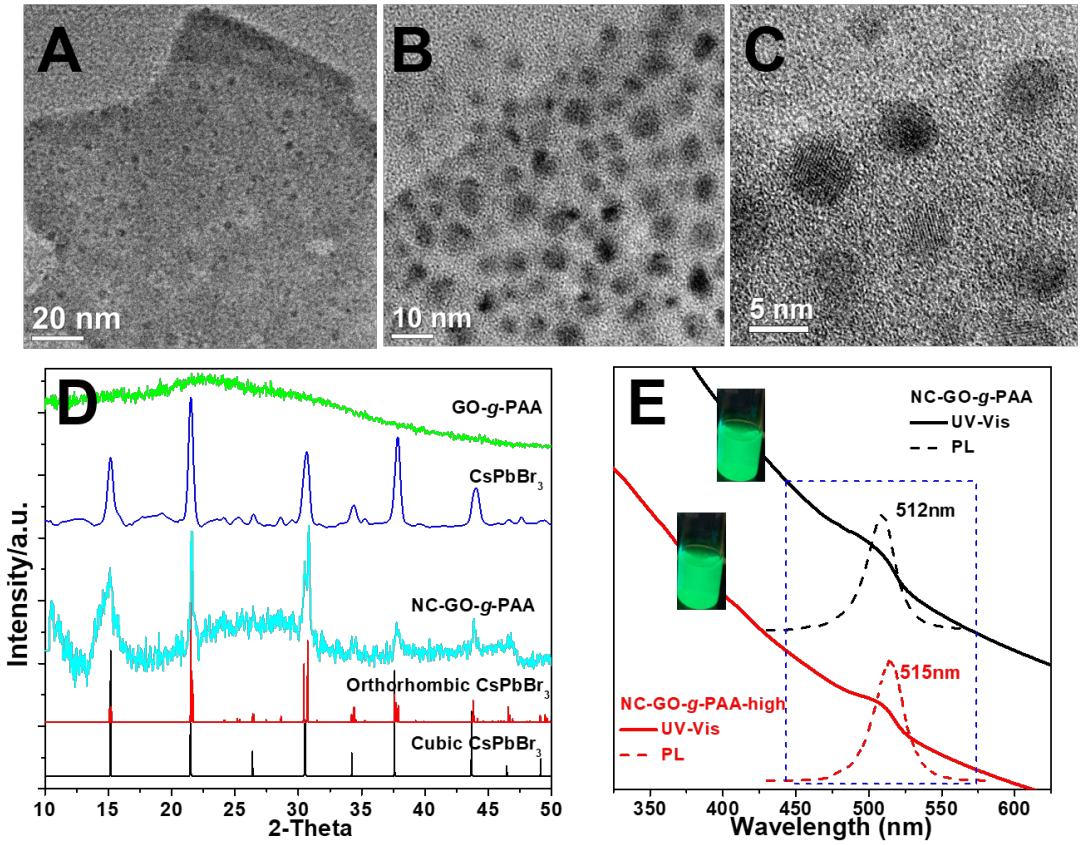

Figure 1. (a) Low- and (b) high- magnification TEM images of the NC-GO-*g*-PAA hybrid. (c) HRTEM of the NCs embedded in the hybrid. (d) XRD pattern (Co K_α) of GO-g-PAA, free $CsPbBr_3$ nanocubes and NC-GO-*g*-PAA hybrid together with the standard XRD patterns of cubic and orthorhombic of $CsPbBr_3$. (e) Optical absorption and PL emission spectra of NC-GO-*g*-PAA and NC-GO-*g*-PAA-high. Insets in (e) are photographs of the colloidal toluene solutions of the hybrids under UV light.

Synthesis of NC-GO-*g*-PAA hybrid was also carried out using GO-*g*-PAA with higher grafting ratio (GO-*g*-PAA-high, 17%) under otherwise identical conditions. TEM analysis revealed that the resulting hybrid is similarly composed of a GO matrix decorated with NCs. The incorporated NCs are slightly more polydisperse and irregular in size, with an average diameter of 10.5±3.7 nm (Figure S5a and S5e). The

crystallinity of QD-GO-*g*-PAA-high was also confirmed by HR-TEM analysis (Figure S5b and S5c). The morphological irregularities suggest that the high concentration of carboxylic acid groups in GO-*g*-PAA-high act cooperatively to influence the crystal nucleation and growth via modulation of the local dielectric environment and precursor concentrations during the kinetic processes that form the NCs.[52,53,54]

While the growth mechanism remains an ongoing subject of study, it is hypothesized that the nucleation starts from the preferential coordination between carboxylate groups on the PAA ligands and the $PbBr_2$ precursors. The carboxylate ligands are known to facilitate uptake of $PbBr_2$ through coordinating interactions, creating kinetically favorable nucleation points. Coexisted with these more tightly bound Pb sources are the unbound $PbBr_2$ that are more mobile in the solution. Once the cesium precursor is injected, free $PbBr_2$ will diffuse to the polymer-bound nucleation sites for subsequent crystal growth. The GO-*g*-PAA nucleated NC growth is presumably competing against the conventional solution based NC growth, the former however is favored as nucleation happens favorably at lower energy interfaces.[55] The unbound NCs from solution-based nucleation could be easily removed by centrifugal purification.

The PAA-initiated NC growth is influenced by the diffusion of free $PbBr_2$ to the nucleation sites. In the case of GO-*g*-PAA-high, the high PAA loading renders these interfacial nucleation sites less accessible to $PbBr_2$ due to denser packing. This leads to a slower nucleation process, which allows the growth of bigger size NCs but with broader size distribution. On the other hand, the concentration of bound $PbBr_2$ may also vary along the PAA polymer chains from the open-end to the GO-bound end.

Such a concentration gradient, which is more pronounced in GO-*g*-PAA-high, could also contribute to the broader size distribution.

UV-Vis absorption and PL emission properties of NC-GO-*g*-PAA and NC-GO-*g*-PAA-high hybrids were evaluated and compared to $CsPbBr_3$ nanocrystals synthesized using traditional oleic acid and oleylamine ligands. The absorption onset and PL emission peak of the free $CsPbBr_3$ nanocrystals (average diameter 9 nm) are ca. 500 nm and 510 nm, respectively, in good agreement with reported values.[17] The absorption and emission spectra of NC-GO-*g*-PAA hybrids exhibit a slight red shift, with an absorption maximum at 512 nm and emission maximum at 515 nm despite their smaller sizes. This is in contrast to the effect of quantum confinement where the absorption and emission spectra undergo a blue shift as the size of NCs decreases. Further red-shifting was observed for the NC-GO-*g*-PAA-high hybrid, with both the absorption and PL emission maxima at 515 nm. This trend may be attributed to the changing of the local dielectric environment around the NCs on the GO-*g*-PAA which depresses the energy of the excited state, leading to a deeper red shift and is consistent with the longer lifetime observed by time-resolved PL studies (Figure S5f).[56, 57] The PLQY (ca. 60%) of the high grafting NC-GO-*g*-PAA-high is lower than that of NC-GO-*g*-PAA (ca. 80%). Higher PAA loading on the GO surface introduces a stronger modification of the local dielectric environment and may significantly impact the crystal nucleation and growth, leading to more irregular size, morphology, and overall lower PLQY. It is worth noting that a PLQY greater than 80% for NC-GO-*g*-PAA is significantly higher than that of previously reported encapsulated NCs, such as APTES-/NH_2-POSS-$CH_3NH_3PbBr_3$ (15-55%),[41] POSS-$CsPbBr_3$ (61%)[40], $CsPbBr_3$@NH_4Br nanocomposite (64.21%)[58] and $CsPbBr_3$@PS composites (64.7%).[59]

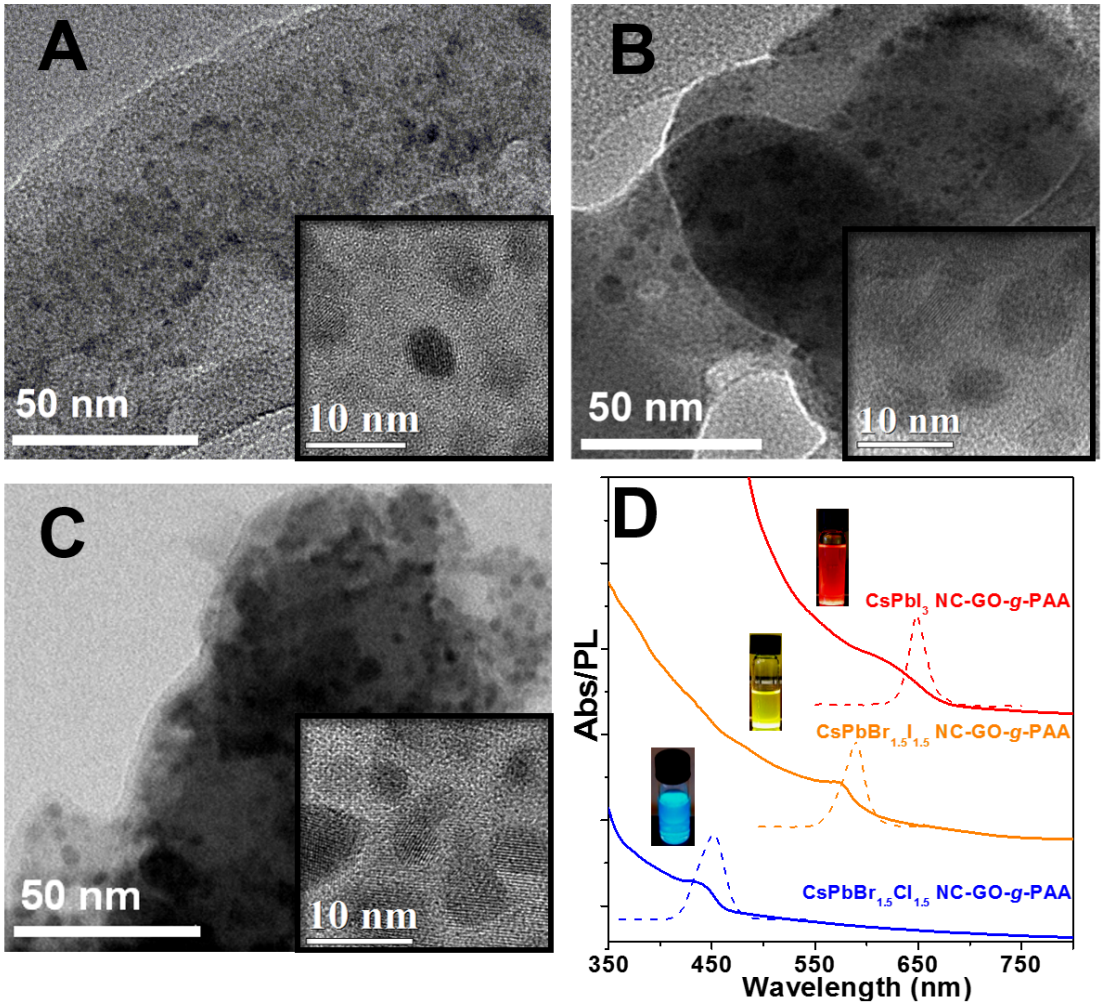

Figure 2. (a) TEM images of blue $CsPbBr_{1.5}Cl_{1.5}$ NC-GO-*g*-PAA, (b) yellow $CsPbBr_{1.5}I_{1.5}$ NC-GO-*g*-PAA, and (c) red $CsPbI_3$ NC-GO-*g*-PAA. Inset images are the corresponding HR-TEM images. (d) UV-vis and PL spectra of $CsPbX_3$ NC-GO-*g*-PAA synthesized with various Cl/Br/I ratios. Photographs of the respective colloidal solutions under UV light are shown in the inset.

The optical properties of the NC-GO-*g*-PAA hybrids can be readily tuned by using different lead halide precursors in the nanocrystal synthesis. As demonstrated here, when mixtures of $PbCl_2/PbBr_2$ (1:1), $PbBr_2/PbI_2$ (1:1), or pure PbI_2 were used instead of $PbBr_2$, colloidal NCs with red, yellow and blue fluorescence were obtained with fair to high PLQY in the range of 50%-80%, respectively assigned to $CsPbBr_{1.5}Cl_{1.5}$ (50%), $CsPbBr_{1.5}I_{1.5}$ (80%) and $CsPbI_3$ (78%) NCs (Figure 2d). Similar to the trend

for free colloidal $CsPbX_3$ NCs,[17, 18, 60] the absorption and emission peaks of NC-GO-*g*-PAA hybrids shift to higher energy and lower energy regions as the Cl and I anions are introduced, respectively. The corresponding TEM images show the formation of uniform NCs embedded in the GO-*g*-PAA matrix, with the average diameters of 8 nm , 11 nm and 12 nm for the mixed $CsPbBr_{1.5}Cl_{1.5}$, $CsPbBr_{1.5}I_{1.5}$ and $CsPbI_3$ NCs, respectively (Figure 2a, 2b and 2c). The bulk crystallinity of the hybrids was confirmed by PXRD studies (Figure S6). The slight shift of the diffraction peaks toward the large and small angle direction when the Cl and I anions introduced is consistent with the formation of the orthorhombic $CsPbCl_{1.5}/Br_{1.5}$ perovskite crystal phases and mixed crystal phases of $CsPbI_3$.[61, 62]

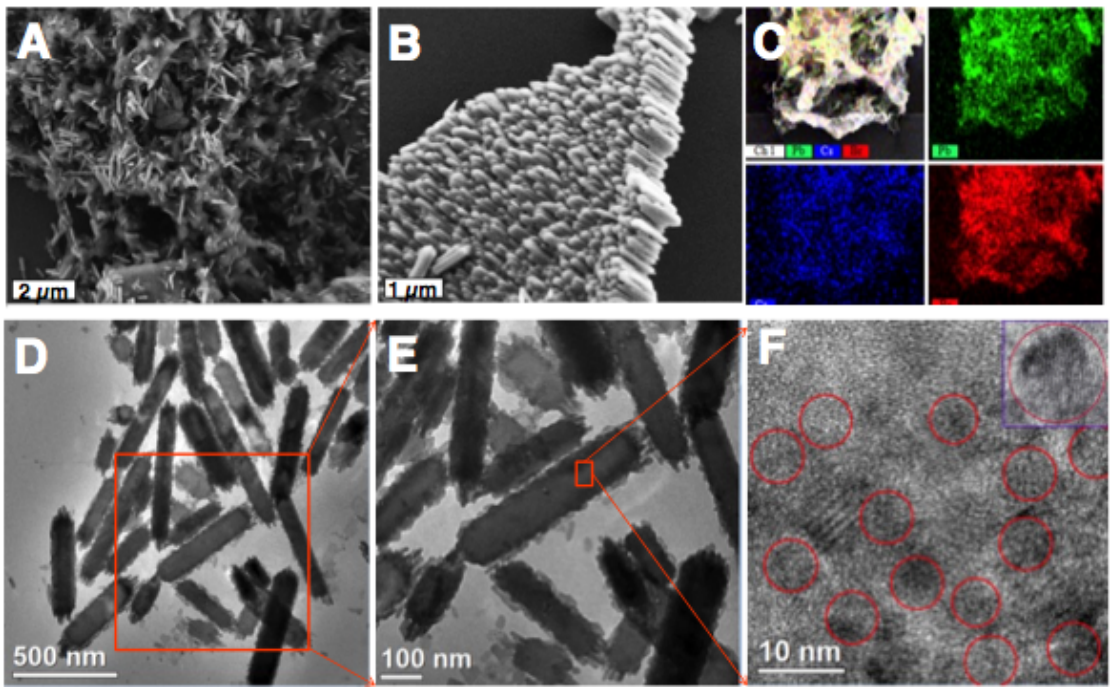

Figure 3. (a, b) SEM images of the self-assembled $CsPbBr_3$ NC-GO-*g*-PAA nanorods. (c) SEM-EDX mapping of Pb (green), Cs (blue) and Br (red) elements in nanorods. Low- (d) and high-magnification (e) TEM images of the self-assembled

nanorods. (f) HR-TEM image showing the crystal lattice of the perovskite $CsPbBr_3$ NCs within nanorods.

Furthermore, addition of the colloidal toluene solution of the $CsPbBr_3$ NC-GO-*g*-PAA hybrid into hexane (Toluene/hexane=1/9, v/v) drove the formation of self-assembled nanorod-shaped suprastructures. Nanorods with diameters between 140 and 175 nm, and lengths between 250 and 600 nm were clearly identified by SEM and TEM. In many areas, vertically oriented arrays of nanorods were formed (Figure 3 and Figure S7). Elemental mapping using energy dispersive X-ray analyzer (EDX) confirmed the presence of Pb, Cs and Br inside the oriented array of nanorods (Figure 3c). HR-TEM images (Figure 3f) of an individual nanorod show the NCs embedded within the nanorod suprastructures. The crystal lattice fringes match well with the pure $CsPbBr_3$ NCs. Further sampling by SEM, TEM and SEM-EDX at different sample locations proved the consistent composition and morphology of the NC-GO-*g*-PAA nanorod suprastructure (Figure S7 and S8).

The hierarchical assembly into nanorod suprastructures from GO-*g*-PAA hybrids may be understood as a solvent polarity driven process. Synthetic polymers and GO have been reported to have different thermal expansion and solubility coefficients.[63] When surface grafted polymers contract upon exposure to anti-solvents, curving of 2D GO sheets may occur in response to the residual stress induced by the physical transition of the morphology of the polymer.[47, 63, 64] The formation of nanorods results from further curling of the curved sheet, which is favored in order to minimize the exposure of the polar PAA chains to the non-polar solvent while maximizing the exposure of GO surface to the solvent. Further control experiments indicated that nanorod arrays were formed from a hexanes/toluene (9/1) solution of GO-*g*-PAA (Figure S9), confirming that the solvent driven assembly of the nanorod is

spontaneous for the GO-*g*-PAA and is independent and unaffected by the surface bound $CsPbBr_3$ nanocrystals. On the other hand, treating a mixed sample of the GO-*g*-PAA and the unbound $CsPbBr_3$ nanocubes under the same conditions only resulted in separate nanorods and non-encapsulated perovskite nanocubes.

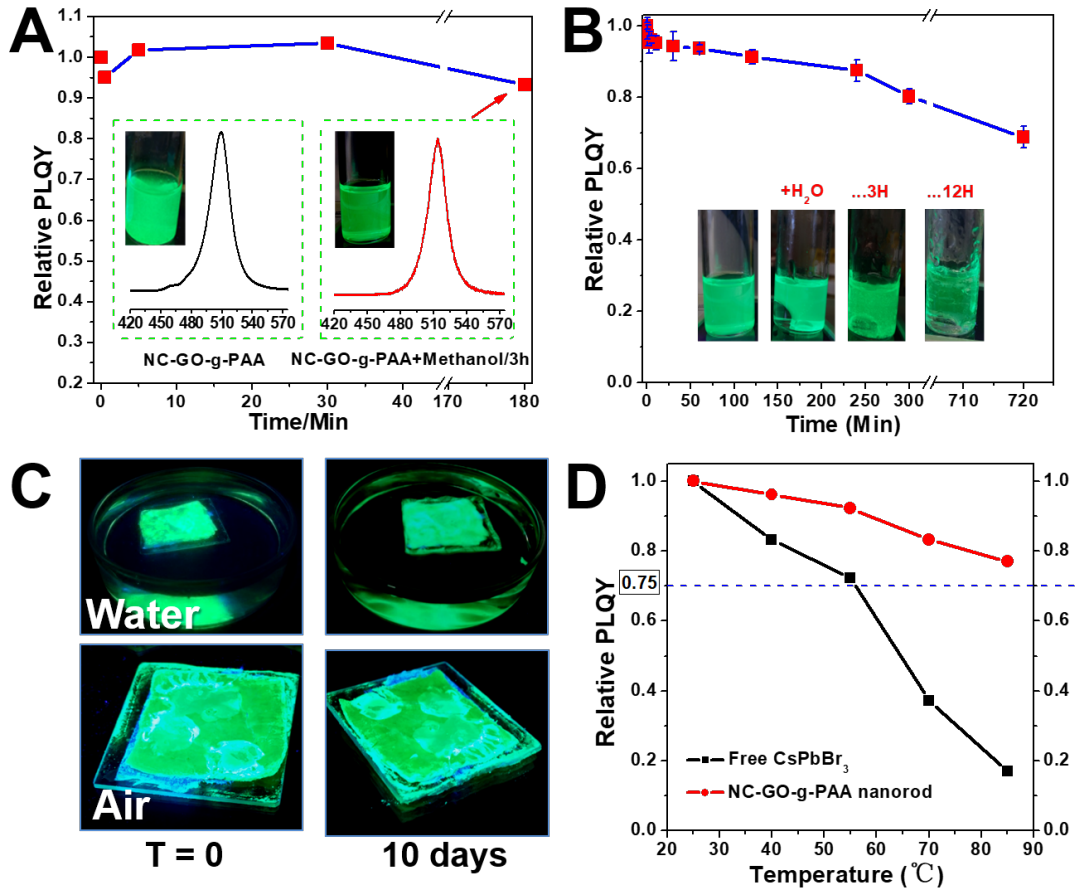

Figure 4. The relative fluorescence intensity of self-assembled NC-GO-*g*-PAA nanostructures over different times upon mixing with a) methanol and b) water. Insets in (a) and (b): optical photographs of methanol and water treated NC-GO-*g*-PAA nanorod solution under UV light. (c): photographs of glass slides coated with NC-GO-*g*-PAA nanorod films after soaking in water or exposure to air for 0 day (left) and 10 days (right). (d) Plot of PLQYs at different temperatures for the hybrid nanorod and free $CsPbBr_3$ NC colloidal solutions (hexane/toluene =1/9, v/v).

The thus formed nanorod suprastructures provide excellent encapsulation of the perovskite NCs, which endow extraordinary stability towards protic solvents such as methanol and water, which are known to degrade perovskite nanocrystals.[41] When methanol was added to a hexane colloidal solution of free $CsPbBr_3$ nanocrystals (10% v/v), its PL intensity decreased by more than 80% within 3 min (Figure S10) and was almost completely quenched in 0.5 h. In contrast, when the colloidal solution of self-assembled $CsPbBr_3$ NC-GO-*g*-PAA nanorods was exposed to the same volume of methanol, the PL intensity remained unchanged after 0.5 h, despite a slight red-shift in both the absorption and emission spectra (Figure 4a), which may be due to solvent induced changes to the local polarity and enhance the dielectric shielding, both of which lower the energy of the excited state. After 3 hours of incubation the sample could still maintain 90% of the original PL intensity.

The stability test was repeated with water in place of methanol. Figure 4b shows the change of PL intensity of self-assembled hybrid nanorod solution over time. After vigorous shaking of the biphasic water/hexane mixture, the emissive color of the NC-GO-*g*-PAA nanorod solution remained similar (see the inset in Figure 4b). The relative PL intensity decreased very slowly over time, retaining 70% of its original value after 12 h exposure to liquid water. In comparison, the non-bound $CsPbBr_3$ immediately loses 50% PL intensity upon mixing with water, and becomes completely non-emissive after 3h (Figure S11). The stability of thin films of $CsPbBr_3$ NC-GO-*g*-PAA nanorods coated on glass slides were also tested by immersing the slides in water or leaving in air for different periods of time (Figure 4c). The thin films remain highly emissive (42% PLQY) after immersion for 40 days and show nearly the same surface morphologies as revealed by SEM studies (Figure S12d). HR-

TEM images (Figure S12e and f) and PL spectra confirm that both the morphology and the emission spectrum of the embedded NCs remain unchanged (Figure S12g).

Additionally, the tendency of the perovskite fluorophores to exchange anions was completely suppressed (Figure S13). No change of emission properties was observed after exposing the hybrid solution to chloride or iodide, in sharp contrast to the free $CsPbBr_3$ NCs. These results collectively demonstrate that the combination of embedding $CsPbBr_3$ NCs in GO-*g*-PAA matrixes and the self-assembled nanorod suprastructure morphology provide a permeation barrier that effectively shields the nanocrystals from environmental agents including solvent and halide ions.

The nanostructured composite also enhanced thermal stability of the nanocrystals. A steep degradation tendency was observed when the colloidal solution of free $CsPbBr_3$ NCs was heated at elevated temperatures for 5 min. At 85 ºC only 17% of its original PL was maintained. In contrast, the colloidal solution of nanorods maintains 77% of its PLQY after heating at 85 ºC for 5 min (Figure 4d).

In summary, PAA grafted graphene oxide was successfully used as a surface ligand on $CsPbX_3$ NCs in place of oleic acid, resulting in ternary NC-GO-*g*-PAA hybrids with uniform NCs distribution in the GO-*g*-PAA matrix, high quantum yields and tunable emission colors. Further self-assembly of the NC-GO-*g*-PAA hybrids was realized upon solvent treatment to give nanorods with diameters in the range of 5 to 12 nm, which provides effective encapsulation of the embedded perovskite NCs. As a result, the NC-GO-*g*-PAA nanorods display significantly improved stability towards protic solvents (methanol and water), suppressed activity towards halide exchange, and enhanced thermal stability compared to free $CsPbBr_3$ NCs. The demonstrated synthetic viability towards ternary pervoskite NC hybrids provides an unprecedented approach to overcoming the major instability challenges for perovskite NC materials.

This composite also has great potential in photocatalysis considering GO's excellent ability to facilitate charge separation and transport.

ASSOCIATED CONTENT

Supporting Information

Synthetic details of GO-*g*-PAA, free $CsPbBr_3$ NCs and NC-GO-*g*-PAA hybrids; TGA curves, XPS spectra, SEM, TEM and HR-TEM images of NC-GO-*g*-PAA hybrids; The stability test of free $CsPbBr_3$ NCs in methanol and water; Anion exchange experiments of the colloidal solutions of free $CsPbX_3$ and NC-GO-*g*-PAA nanorods.

AUTHOR INFORMATION

Corresponding Author

*Email: yliu@lbl.gov, heling@mail.xjtu.edu.cn

Author Contributions

The manuscript was written through contributions of all authors. All authors have given approval to the final version of the manuscript.

Notes

The authors declare no competing financial interest

ACKNOWLEDGMENT

This work was primarily supported by the U.S. Department of Energy, Office of Science, Office of Basic Energy Sciences, Materials Sciences and Engineering Division, under Contract No. DE-AC02-05-CH11231 within the Inorganic/Organic Nanocomposites Program (KC3104) (materials synthesis, sample preparation, and analysis). Work at the Molecular Foundry was supported by the Office of Science,

Office of Basic Energy Sciences, of the U.S. Department of Energy under Contract No. DE-AC02-05CH11231. This work was also supported by the National Natural Science Foundation of China (NSFC Grants 51373133, 51573145). The authors also wish to express their gratitude to the MOE Key Laboratory for Nonequilibrium Condensed Matter and Quantum Engineering of Xi'an Jiaotong University. The authors thank Zeke Liu and Paul Alivisatos from University of California, Berkeley for help with TEM characterizations, and Guijiang Zhou, Yanfeng Zhang and Youshen Wu from Xi'an Jiaotong University for helpful discussions.

References

1. Green, M. A.; Ho-Baillie, A.; Snaith, H. J. *Nat. Photonics* **2014,** 8, 506-514.
2. Yakunin, S.; Protesescu, L.; Krieg, F.; Bodnarchuk, M. I.; Nedelcu, G.; Humer, M.; De Luca, G.; Fiebig, M.; Heiss, W.; Kovalenko, M. V. *Nat. Commun.* **2015,** 6, 8056-8063
3. Jeon, N. J.; Noh, J. H.; Yang, W. S.; Kim, Y. C.; Ryu, S.; Seo, J.; Seok, S. I. *Nature* **2015,** 517, 476-480.
4. Swarnkar, A.; Chulliyil, R.; Ravi, V. K.; Irfanullah, M.; Chowdhury, A.; Nag, A. *Angew. Chem. Int. Ed. Engl.* **2015,** 54, 15644-15648.
5. Zhang, N.; Yang, M. Q.; Liu, S.; Sun, Y.; Xu, Y. J. *Chemical reviews* **2015,** 115, 10307-77.
6. Yuan, Z.; Zhou, C.; Tian, Y.; Shu, Y.; Messier, J.; Wang, J. C.; van de Burgt, L. J.; Kountouriotis, K.; Xin, Y.; Holt, E.; Schanze, K.; Clark, R.; Siegrist, T.; Ma, B. *Nat. Commun.* **2017,** 8, 14051-14058..
7. Veldhuis, S. A.; Boix, P. P.; Yantara, N.; Li, M.; Sum, T. C.; Mathews, N.; Mhaisalkar, S. G. *Adv. Mater.* **2016,** 28, 6804-6834.
8. Song, J.; Li, J.; Li, X.; Xu, L.; Dong, Y.; Zeng, H. *Adv. Mater.* **2015,** 27, 7162-7167.
9. Palazon, F.; Di Stasio, F.; Akkerman, Q. A.; Krahne, R.; Prato, M.; Manna, L. *Chem.Mater.* **2016,** 28, 2902-2906.
10. Yantara, N.; Bhaumik, S.; Yan, F.; Sabba, D.; Dewi, H. A.; Mathews, N.; Boix, P. P.; Demir, H. V.; Mhaisalkar, S. *J. Phys. Chem. Lett.* **2015,** 6, 4360-4364.
11. Eaton, S. W.; Lai, M.; Gibson, N. A.; Wong, A. B.; Dou, L.; Ma, J.; Wang, L. W.; Leone, S. R.; Yang, P. *Proc. Natl Acad. Sci. U. S. A.* **2016,** 113, 1993-1998.
12. Sharenko, A.; Toney, M. F. *J. Am. Chem. Soc.* **2016,** 138, 463-470.
13. Yi, C.; Luo, J.; Meloni, S.; Boziki, A.; Ashari-Astani, N.; Grätzel, C.; Zakeeruddin, S. M.; Röthlisberger, U.; Grätzel, M. *Energy Environ. Sci.* **2016,** 9, 656-662.
14. Song, J.; Xu, L.; Li, J.; Xue, J.; Dong, Y.; Li, X.; Zeng, H. *Adv. Mater.* **2016,** 28, 4861-4869.

15. Ramasamy, P.; Lim, D. H.; Kim, B.; Lee, S. H.; Lee, M. S.; Lee, J. S. *Chem. Commun.* **2016,** 52, 2067-2070.
16. Seth, S.; Mondal, N.; Patra, S.; Samanta, A. *J. Phys. Chem. Lett.* **2016,** 7, 266-271.
17. Protesescu, L.; Yakunin, S.; Bodnarchuk, M. I.; Krieg, F.; Caputo, R.; Hendon, C. H.; Yang, R. X.; Walsh, A.; Kovalenko, M. V. *Nano Lett.* **2015,** 15, 3692-3696.
18. Nedelcu, G.; Protesescu, L.; Yakunin, S.; Bodnarchuk, M. I.; Grotevent, M. J.; Kovalenko, M. V. *Nano Lett.* **2015,** 15, 5635-5640.
19. Aharon, S.; Etgar, L. *Nano Lett.* **2016,** 16, 3230-3235.
20. Zhu, F.; Men, L.; Guo, Y.; Zhu, Q.; Bhattacharjee, U.; Goodwin, P. M.; Petrich, J. W.; Smith, E. A.; Vela, J. *ACS Nano* **2015,** 9, 2948-2959.
21. Pan, A.; He, B.; Fan, X.; Liu, Z.; Urban, J. J.; Alivisatos, A. P.; He, L.; Liu, Y. *ACS Nano* **2016,** 10, 7943-7954.
22. Sun, S.; Yuan, D.; Xu, Y.; Wang, A.; Deng, Z. *ACS Nano* **2016,** 10, 3648-3657.
23. Bekenstein, Y.; Koscher, B. A.; Eaton, S. W.; Yang, P.; Alivisatos, A. P. *J. Am. Chem. Soc.* **2015,** 137, 16008-16011.
24. Koolyk, M.; Amgar, D.; Aharon, S.; Etgar, L. *Nanoscale* **2016,** 8, 6403-6409.
25. Samadi Khoshkhoo, M.; Maiti, S.; Schreiber, F.; Chasse, T.; Scheele, M. *ACS Appl. Mater. Interfaces* **2017,** 9, 14197-14206.
26. Raja, S. N.; Bekenstein, Y.; Koc, M. A.; Fischer, S.; Zhang, D.; Lin, L.; Ritchie, R. O.; Yang, P.; Alivisatos, A. P. *ACS Appl. Mater. Interfaces* **2016,** 8, 35523-35533.
27. Kim, Y.; Yassitepe, E.; Voznyy, O.; Comin, R.; Walters, G.; Gong, X.; Kanjanaboos, P.; Nogueira, A. F.; Sargent, E. H. *ACS Appl. Mater. Interfaces* **2015,** 7, 25007-25013.
28. Christians, J. A.; Miranda Herrera, P. A.; Kamat, P. V. *J. Am. Chem. Soc.* **2015,** 137, 1530-1538.
29. Wang, H. C.; Lin, S. Y.; Tang, A. C.; Singh, B. P.; Tong, H. C.; Chen, C. Y.; Lee, Y. C.; Tsai, T. L.; Liu, R. S. *Angew. Chem. Int. Ed. Engl.* **2016,** 55, 7924-7929.
30. Beal, R. E.; Slotcavage, D. J.; Leijtens, T.; Bowring, A. R.; Belisle, R. A.; Nguyen, W. H.; Burkhard, G. F.; Hoke, E. T.; McGehee, M. D. *J. Phys. Chem. Lett.* **2016,** 7, 746-751.
31. Jiang, Q.; Rebollar, D.; Gong, J.; Piacentino, E. L.; Zheng, C.; Xu, T. *Angew. Chem. Int. Ed. Engl.* **2015,** 54, 7617-20.
32. Pathak, S.; Sakai, N.; Wisnivesky Rocca Rivarola, F.; Stranks, S. D.; Liu, J.; Eperon, G. E.; Ducati, C.; Wojciechowski, K.; Griffiths, J. T.; Haghighirad, A. A.; Pellaroque, A.; Friend, R. H.; Snaith, H. J. *Chem. Mater.* **2015,** 27, 8066-8075.
33. Wang, Y.; He, J.; Chen, H.; Chen, J.; Zhu, R.; Ma, P.; Towers, A.; Lin, Y.; Gesquiere, A. J.; Wu, S. T.; Dong, Y. *Adv. Mater.* **2016,** 28, 10710-10717.
34. Malgras, V.; Tominaka, S.; Ryan, J. W.; Henzie, J.; Takei, T.; Ohara, K.; Yamauchi, Y. *J. Am. Chem. Soc.* **2016**, 138, 13874-13881.
35. Dirin, D. N.; Protesescu, L.; Trummer, D.; Kochetygov, I. V.; Yakunin, S.; Krumeich, F.; Stadie, N. P.; Kovalenko, M. V. *Nano Lett.* **2016,** 16, 5866-5874.
36. Ruan, L.; Shen, W.; Wang, A.; Zhou, Q.; Zhang, H.; Deng, Z. *Nanoscale* **2017,** 9, 7252-7259.
37. Liu, Z.; Bekenstein, Y.; Ye, X.; Nguyen, S. C.; Swabeck, J.; Zhang, D.; Lee, S. T.; Yang, P.; Ma, W.; Alivisatos, A. P. *J. Am. Chem. Soc.* **2017,** 139, 5309-5312.
38. Ruan, L.; Shen, W.; Wang, A.; Xiang, A.; Deng, Z. *J. Phys. Chem. Lett.* **2017,** 8, 3853-3860.
39. Hai, J.; Li, H.; Zhao, Y.; Chen, F.; Peng, Y.; Wang, B. *Chem. Commun.* **2017**, 53, 5400-5403.

40. Huang, H.; Chen, B.; Wang, Z.; Hung, T. F.; Susha, A. S.; Zhong, H.; Rogach, A. L. *Chem. Sci.* **2016,** 7, 5699-5703.
41. Luo, B.; Pu, Y. C.; Lindley, S. A.; Yang, Y.; Lu, L.; Li, Y.; Li, X.; Zhang, J. Z. *Angew. Chem. Int. Ed.* **2016**, 128, 9010-9014.
42. Jiang, Z. J.; Kelley, D. F. *J. Phys. Chem. C* **2012,** 116, 12958-12968.
43. Virgili, T.; Calzolari, A.; Suárez López, I.; Vercelli, B.; Zotti, G.; Catellani, A.; Ruini, A.; Tassone, F. *J. Phys. Chem. C* **2013,** 117, 5969-5974.
44. Jurow, M.; Manichev, V.; Pabon, C.; Hageman, B.; Matolina, Y.; Drain, C. M. *Inorg. Chem.* **2013,** 52, 10576-10582.
45. Yao, X.; Zhao, Y. *Chem* **2017,** 2, 171-200.
46. Cho, E. S.; Ruminski, A. M.; Aloni, S.; Liu, Y. S.; Guo, J.; Urban, J. J. *Nat. Commun.* **2016,** 7, 10804-10810.
47. Su, Y.; Kravets, V. G.; Wong, S. L.; Waters, J.; Geim, A. K.; Nair, R. R. *Nat. Commun.* **2014,** 5, 4843-4846.
48. Hou, S.; Guo, Y.; Tang, Y.; Quan, Q. *ACS Appl. Mater. Interfaces* **2017,** 9, 18417-18422.
49. Xu, Y. F.; Yang, M. Z.; Chen, B. X.; Wang, X. D.; Chen, H. Y.; Kuang, D. B.; Su, C. Y. *J. Am. Chem. Soc.* **2017**, 139, 5660-5663.
50. Tang, X.; Zu, Z.; Zang, Z.; Hu, Z.; Hu, W.; Yao, Z.; Chen, W.; Li, S.; Han, S.; Zhou, M. *Sens. Actuators B: Chem.* **2017,** 245, 435-440.
51. Li, G. L.; Liu, G.; Li, M.; Wan, D.; Neoh, K. G.; Kang, E. T. *J. Phys. Chem. C* ***2010,*** 10, 114, 12742-12748.
52. Van Embden, J.; Mulvaney, P. *Langmuir* **2005,** 21, 10226-10233.
53. Burda, C.; Chen, X.; Narayanan, R.; El-Sayed M. A. *Chem. Rev.* **2005,** 105, 1025-1102.
54. Manna, L.; Scher, E. C.; Alivisatos, A. P. *J. Am. Chem. Soc.* **2000,** 122, 12700-12706.
55. De Yoreo, J. J.; Vekilov, P. G. *Rev. Mineral. Geochem.* **2003**, 54, 57-93.
56.Weiss, M. T. F. a. E. A. *ACS nano* **2010,** 4, 3195-3200.
57. Wolcott, A.; Doyeux, V.; Nelson, C. A.; Gearba, R.; Lei, K. W.; Yager, K. G.; Dolocan, A. D.; Williams, K.; Nguyen, D.; Zhu, X. Y. *J. Phys. Chem. Lett.* **2011,** 2, 795-800.
58. Lou, S.; Xuan, T.; Yu, C.; Cao, M.; Xia, C.; Wang, J.; Li, H. *J. Mater. Chem. C* **2017,** 5, 7431-7435.
59. Wei, Y.; Deng, X.; Xie, Z.; Cai, X.; Liang, S.; Ma, P. a.; Hou, Z.; Cheng, Z.; Lin, J. *Adv. Funct. Mater.* **2017**, 1703535-1703542.
60. Akkerman, Q. A.; D'Innocenzo, V.; Accornero, S.; Scarpellini, A.; Petrozza, A.; Prato, M.; Manna, L. *J. Am. Chem. Soc.* **2015,** 137, 10276-10281.
61. Wang, C.; Chesman, A. S.; Jasieniak, J. J. *Chem. Commun.* **2016,** 53, 232-235.
62. Monshi, A.; Foroughi, M. R.; Monshi, M. R. *World J. Nano Sci. Eng.* **2012,** 02, (03), 154-160.
63. Li, C.; Koslowski, M.; Strachan, A. *Nano Lett.* **2014,** 14, 7085-7089.
64 Amadei, C. A.; Stein, I. Y.; Silverberg, G. J.; Wardle, B. L.; Vecitis, C. D. *Nanoscale* **2016,** 8, 6783-6791.

TOC Graphics

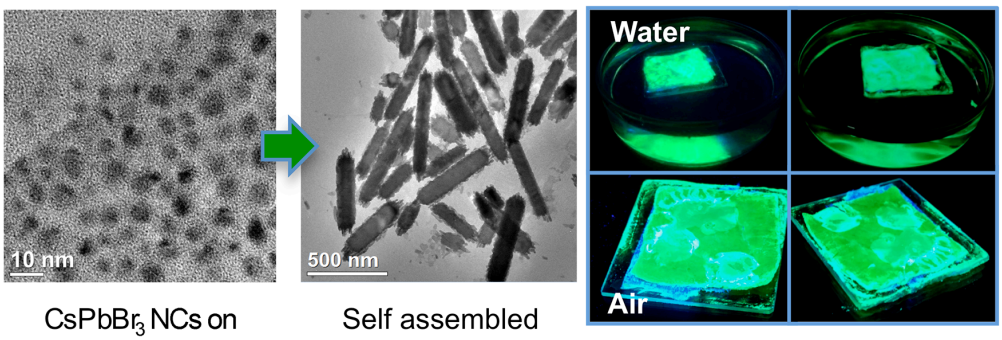

$CsPbBr_3$ NCs on GO–*g*-PAA

Self assembled nanorods

T=0

10 days